Scanning tunneling microscopy of the subsurface structures of tungsten ditelluride and molybdenum ditelluride

S. L. Tang, R. V. Kasowski, and B. A. Parkinson

E. I. DuPont de Nemours and Co., Central Research and Development Department, Experimental Station, Wilmington, Delaware 19898

The surface structure of the van der Waals faces of tungsten ditelluride (WTe_2) and molybdenum ditelluride ($2H$-$MoTe_2$) have been studied with scanning tunneling microscopy (STM). The hexagonal symmetry observed on the $2H$-$MoTe_2$ surface is similar to that observed previously on other transition-metal dichalcogenides. On WTe_2, which has a distorted layered structure due to the pairing of the metal atoms, the scanning tunneling micrographs distinctly show the dominance of the metal. Buckled, zig-zag chains of paired atomic rows, which are the signature of the tungsten layer, are observed. These results show for the first time that subsurface atoms can be imaged with the STM. The corrugated surface tellurium layer could not be identified unambiguously in two-dimensional scans. These results are surprising because a first-principles pseudofunction calculation of the surface-electronic charge density around the Fermi energy of the WTe_2 surface shows that the calculated spatial distribution of the charge density at the surface has the characteristics of the topmost Te atoms. The experimental observations suggest that, unlike the case of graphite images, a direct comparison of the STM image of this surface with calculated surface charge density is not possible. These observations further suggest that the hexagonal symmetry observed in $MoTe_2$ and other transition-metal dichalcogenides is also due to the metal layer rather than the surface chalcogenides.

The layered transition-metal dichalcogenides have been extensively studied because of their many novel properties, ranging from superconductivity to charge-density waves.[1] The van der Waals surfaces of these compounds have also recently been widely studied with scanning tunneling microscopy (STM). The flatness, the inertness even in water,[2] and also the ease of obtaining nearly defect-free, atomically clean surfaces make these materials extremely suitable for STM studies and applications. The charge-density waves in several of these compounds,[3] the surface structures of $NbSe_2$,[4] and MoS_2 (Refs. 5–7) have been imaged with atomic resolution. In all of these STM studies, the surfaces have shown the expected bulk-like hexagonal-close-packed structure, since the van der Waals surface is fully bonded and does not reconstruct. In spite of the lack of dangling bonds and surface reconstructions which should simplify the interpretation of the STM images, the interpretation of the hexagonal image remains uncertain. In some of these studies, the observed hexagonal symmetry has been attributed to the chalcogenide atoms since the chalcogenides are the top surface layer. A faint, secondary hexagon in some of these grey-scale micrographs has been assigned to be the atomic positions of the subsurface metal atoms.[4,5] In another study,[6] the surface hexagonal symmetry was argued to be due to the metal atoms as a result of the metal d_{z^2} orbitals protruding vertically to the surface to provide the electronic states for electron tunneling. A scanning-tunneling-spectroscopic study of the $NbSe_2$ surface in ambient atmosphere concludes that both the Nb and Se atoms can be observed depending on the bias voltage

used.[8] This conclusion, however, is not consistent with the observation of simultaneous bright and faint hexagons at a single bias voltage. Since the surface chalcogenide layer and the second layer of metal atoms of these compounds have the same hexagonal symmetry, STM images of these surfaces cannot easily distinguish the two chemically distinct layers.

In this paper we address the problem of whether the surface chalcogenide layer or the subsurface metal layer is imaged with the STM by studying two structurally different compounds, WTe_2 and $MoTe_2$. The structures of these two compounds are shown in Fig. 1. Low-energy electron-diffraction studies of the surfaces of these compounds also show the patterns expected from their bulk structures. Figure 1(a) shows the computer-generated top-view structure of WTe_2. The structural parameters used in the construction of the model are from an x-ray-diffraction study of the bulk WTe_2.[9] This compound differs from the other metal dichalcogenides studied to date in that the metal atoms have a distorted octahedral coordination. The distortion has the effect of shifting one tungsten atom 0.95 Å horizontally from the center of the unit cell and also 0.21 Å vertically from the remaining W atoms. The result is that every two rows of W atoms pair to form zig-zag and slightly buckled chains. Consequently, the tellurium layers become slightly corrugated, i.e., alternate rows of tellurium atoms are displaced 0.61 Å upward relative to the lower rows of tellurium atoms. The surface unit cell is rectangular with dimensions of 6.3×3.5 Å^2. Figure 1(b) shows the side view of two sandwich layers which highlight the buckling aspect of
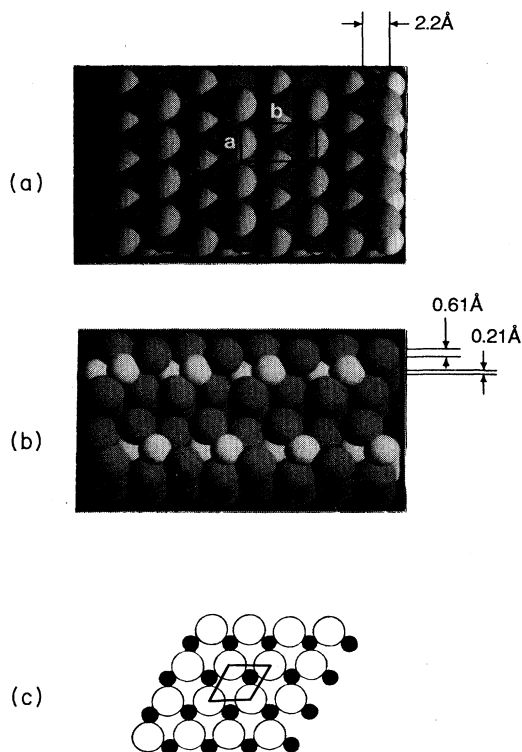
(a)

(b)

(c)

FIG. 1. (a) A computer model of the WTe$_2$ surface with shadowing to highlight the corrugated nature of the Te atoms. Dark balls, Te; light balls, W. Surface unit-cell vector $a = 3.5$ Å, $b = 6.3$ Å. The zig-zag chains of tungsten atoms are denoted by the dashed line. (b) A side view of two computer-generated WTe$_2$ sandwich layers to show the buckling of the paired tungsten rows and the corrugated Te surface layer. (c) The atomic arrangement of the 2H-MoTe$_2$ surface. Open circle, surface Te; solid circle, subsurface Mo. The nearest-neighbor distance is 3.5 Å.

the structures. Since the surface and second layer in WTe$_2$ have different structures, STM images should differentiate the top layer from the second layer.

The MoTe$_2$ surface was chosen to study for comparison. The structural symmetry of MoTe$_2$ in Fig. 1(c) is similar to that of the widely studied 2H-MoS$_2$. The layered structure is made up of Te-Mo-Te sandwiches with the Mo atom having trigonal prismatic coordination. The Te atoms of the van der Waals surfaces and the Mo atoms in between both have hexagonal arrangements. The nearest-neighbor distance within the Mo and the Te layers is 3.5 Å.

The experiment was carried out in ambient atmosphere with two different scanning tunneling microscopes. The first microscope is of our own design and has·been described elsewhere.[10] The second microscope is a commercial instrument.[11] A bench-top vibration-isolation platform was used for building vibration isolation. An aluminum enclosure lined with vibration-damping sheets was used for electrical and acoustic noise isolation. The tunneling images were obtained with the STM operating in both the constant-current and constant-height modes.

Tips used were either electrochemically etched tungsten wires or mechanically sharpened platinum and/or iridium wires. Results obtained from different operational modes and different tips are essentially the same.

The WTe$_2$ and MoTe$_2$ samples were grown by iodine-vapor transport. Flat, shiny, thin crystals were chosen for these experiments. The MoTe$_2$ samples are n-doped semiconductors with an indirect band gap of 0.9 eV. The doping level has not been measured, but the conductivity of the samples is such that the electrical connection from the microscope has to be made directly on the sample surface when a tunneling bias of ~ 1 V is used. WTe$_2$ is metallic. X-ray-photoemission experiments demonstrate that a freshly cleaved surface of MoTe$_2$ remains atomically clean for at least 24 h in air, whereas WTe$_2$ surfaces show evidence for the onset of oxidation after only a few minutes of exposure to air. The effect of oxygen on the STM images of WTe$_2$ surfaces has also been observed.[12] All results reported here were taken within 3 h of cleaving a new surface and during this time, large clean areas (over 1000 Å^2) were readily located.

Figure 2 shows two images obtained on the WTe$_2$ sur-

(a)

(b)

(c)
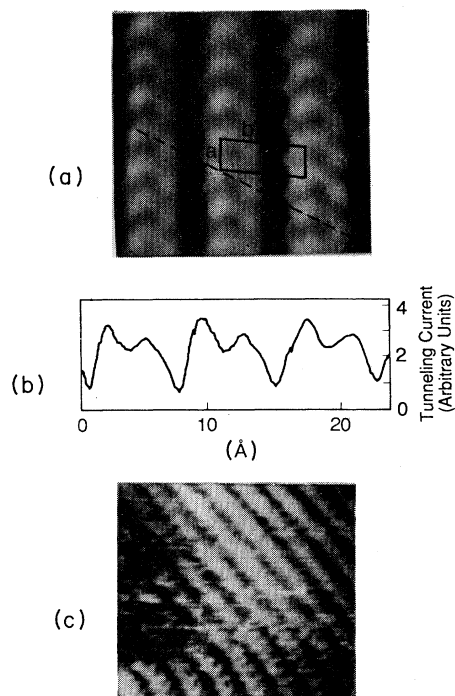
FIG. 2. (a) A (20×25)-Å^2 constant-height scan of the WTe$_2$ surface. The surface unit cell is outlined. The dashed line shows the location of the cross-section line scan shown in (b). (b) The cross-section line scan through the paired, zig-zag rows in (a). (c) A (50×50)-Å^2 scan of the WTe$_2$ surface taken with a constant current. Horizontal streaks along the x-scan directions indicate changes in the tip resolution. The zig-zag pattern of the W layer is clearly observed at the lower part of the scan, but no longer distinguishable toward the top of the scan. The dark areas with atomic features superimposed on them on the left of the scan are defects due to oxygen contamination.

face. The features shown in these images are representative of the hundreds of images taken with different scan directions and with a sample bias range of ± 0.8 V. Images taken with a negative sample bias show more distinct corrugations than those taken with a positive sample bias. The periodicities of 6.3 and 3.5 Å along the b and a axes, respectively, are observed in all two-dimensional (2D) scans.

Figure 2(a) shows a (20×25)-Å^2 scan taken with the constant-height mode. The average current was 1.7 nA and the sample bias was -0.13 V. There are three distinct corrugations in the unit cell. The white-grey pairing due to buckling and the zig-zag pattern are exactly the same as the W layer in the model in Fig. 1(a). The distortion of the rectangular unit cell to a parallelogram is probably due to the combined effects of drift and a slight nonorthogonality of the scan axes. Figure 2(b) shows a section through the zig-zag chains. The sectional line scan shows more quantitatively the paired and buckled nature of the tungsten chain. The separation between the local maxima of the paired row is 2.9 ± 0.1 Å, which agrees well with the 2.8-Å separation between the paired rows in the model. To demonstrate that the image in Fig. 2(a) requires exceptionally good tip resolution, Fig. 2(c) is a (50×50)-Å^2 scan that shows the paired, zig-zag tungsten rows in the lower part of the picture and merged rows towards the top. The sample bias was -0.4 V and the tunneling current was constant at 0.3 nA. Between the two regions, there are horizontal streaks that were caused by dc jumps in the feedback-loop electronics most likely due to changes in the tip. Apparently, the changes in the tip decrease its resolution during the scan such that the zig-zag pattern can no longer be resolved. It should be noted that observation of the fine structure of the zig-zag chain requires an extremely demanding lateral resolution of about 1 Å.

Figure 3(a) shows an image of MoTe$_2$ in a (15×15)-Å^2 scan taken with a sample bias of -0.67 V and a constant tunneling current of 0.2 nA. In this grey-scale micrograph the hexagonal symmetry of the surface is readily observed. The secondary hexagon attributed to a different set of atoms is seen in some of our images. Such an image is shown in Fig. 3(b). The scan area is 16×16 Å^2. The sample bias was $+0.2$ V and the current was constant at 0.2 nA. However, in view of the problems with the tip, it is difficult to rule out that the extra features in those picture are due to an asymmetric tip.

The results from the WTe$_2$ surface clearly show the paired zig-zag chains characteristic of the tungsten layer. These results therefore unambiguously demonstrate for the first time that it is possible for the STM to image subsurface atoms. Although there are some faint indications of additional features in the images, the symmetrically corrugated surface of the Te atoms cannot be unambiguously identified in 2D scans.

Previous STM studies on transition-metal dichalcogenide surfaces sometimes invoked the bulk band calculations[5] or the molecular-orbital bonding scheme[6] of these compounds to interpret the STM images. Empirical tight-binding calculations[13] on the bulk-electronic properties of WTe$_2$ and MoTe$_2$ indicate that a substantial part of the density of states around the Fermi level is indeed derived from the metal d electrons. However, the covalent character of the tungsten-tellurium bond results in heavy mixing of the metal d electrons with the tellurium p electrons, which then contribute considerably to the density of states about the Fermi energy. A first-principles pseudofunction calculation[14] of the density of states of WTe$_2$ also shows essentially the same features. Thus the energy consideration of the density of states alone cannot explain the observation of metal atoms rather than the chalcogenide layer in the STM images. It has been argued in the case of 2H-MoS$_2$ that the metal non-bonding d_{z^2} orbital, which occupies the top of the valence band in the group-VI metal dichalcogenides, is responsible for providing the states for tunneling because the shape of the d_{z^2} orbital favors the extension of the electronic state beyond the air-surface interface.[6] The same argument cannot be applied without caution to the WTe$_2$ case because the splitting of the d orbitals of the distorted octahedral coordination of the W atom is different from that of the trigonal prismatic case. In WTe$_2$ the d_{z^2} orbital is not singly degenerate as in the trigonal prismatic coordination, but rather is triply degenerate with the $d_{x^2-y^2}$ and d_{xy} orbitals and therefore should mix with the latter two orbitals. The component of the d_{z^2} state that protrudes into the air-surface interface is perhaps not as strong as in the trigonal prismatic coordination. Moreover, the d orbitals at the top of the valence band of
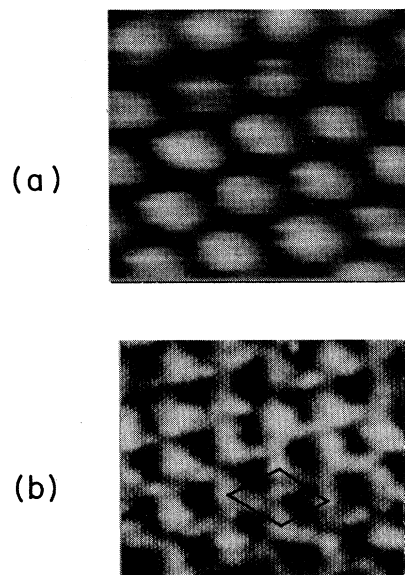

(a)

(b)

FIG. 3. STM images of the 2H-MoTe$_2$ surface taken with the constant-current mode. (a) A (15×15)-Å^2 scan showing the familiar hexagonal symmetry. (b) A (16×16)-Å^2 scan showing additional features attributable to atoms from a different layer. A unit cell is drawn to show the position of the additional feature.

MoTe$_2$ and close to the Fermi energy of WTe$_2$ are more heavily mixed with the tellurium p orbitals than the more ionic dichalcogenide, 2H-MoS$_2$.[13,14] These considerations point to the necessity of more detailed calculations in order to understand why the tungsten atoms show clearly in the STM results, whereas the Te layer is difficult to distinguish.

The calculated quantity most relevant to explain STM images is the surface local density of states, or, in some cases, the spatial distribution of the total valence charge density at the surface. The surface local density of states, and in systems where the Fermi surface is extended, the total charge density, have been shown to be proportional to the tunneling conductance.[15] On another layered material, highly oriented pyrolytic graphite, the influence of subsurface atoms on STM images was previously justified by the surface total charge-density calculations.[16] The tunneling images of graphite show only three atomic positions for the familiar surface hexagon. The interpretation is that only alternate C atoms in the hexagon have neighbors in the layer directly underneath. The bonding between the interlayer nearest neighbors affects the surface charge density such that three of the six atoms appear to be higher.[16,17] Using the same approach, we perform a first-principles pseudofunction calculation of the spatial distribution of the surface charge density as a function of distance from the surface. The pseudofunction method for electronic structures has been successfully applied to several systems, including a surface-adsorbate system[18] and another layered compound, the high-T_c superconductor Bi$_2$Sr$_2$CaCu$_2$O$_8$.[19] The calculation was carried out using a slab containing two Te-W-Te sandwiches. Figure 4 shows the spatial distribution of the surface charge density at $\pm$0.45 eV with respect to the Fermi energy and 1.6 Å above the topmost Te plane. It is clear that the surface charge density has a spatial distribution centered around the topmost Te atoms. Slices of the density-of-states plot taken with energy windows of $E = +0.45$ eV and -0.45 eV at various distances above the Te atoms show essentially the same spatial distribution. Comparing the experimental observations to these calculated results, it is obvious that a straightforward interpretation of the results based on the surface total charge density is not valid for this surface. We also quantitatively rule out the highly improbable (because of the fully bonded nature of the surface) possibility of a gross surface reconstruction of the Te layer. A total-energy calculation of the assumed structure of the Te layer that would give rise to the observed image is less stable than the unreconstructed surface by 1 eV. It is possible that a detailed evaluation of the tunneling matrix element, specifically a detailed knowledge of the wave functions responsible for tunneling, is necessary for understanding the experimental observations.

The STM images observed in this experiment, though not understood in terms of the conventional charge-density picture, do allow us to make the following suggestion. In the present case of WTe$_2$, where the stronger covalency and less-well-defined d_{z^2} characteristics should favor the detection of the surface chalcogenide layer with the STM, the subsurface metal layer still dominates. It is

then reasonable to assert that the primary hexagons observed in the more ionic MoTe$_2$ and MoS$_2$, especially when tunneling from the valence band, are also due to the metal layer rather than the chalcogen layer. The same argument should also apply to NbSe$_2$, a metallic compound where the Nb atom also has trigonal prismatic coordination.

It is interesting at this point to compare the observations and interpretations of the STM images of the WTe$_2$ and MoTe$_2$ surfaces to other heteroatomic surfaces. Recently, Marchon et $al.$ observed in their STM study of the spatial distribution of the tunneling barrier heights the hexagonally packed S atoms in the chemisorbed S layer on a Mo(100) surface.[20] In another STM study of the reconstructed As-terminated GaAs(001) surface, it is also concluded that only the top As layer contributes to the STM images.[21] The bonding structures of these two examples are drastically differently from those of the transition-metal dichalcogenide surfaces. It seems possible that the dominance of the second-layer atoms in STM images is probably specific to the transition-metal dichalcogenides where the surface layer is fully bonded with the bonding electrons mostly confined in and below the surface. Indeed, the observation of bulklike σ-bonding states in STM has been extremely rare. The only example is found in the image of the backbonds in Si(111)-7$\times$7 using the current-imaging techniques.[22]
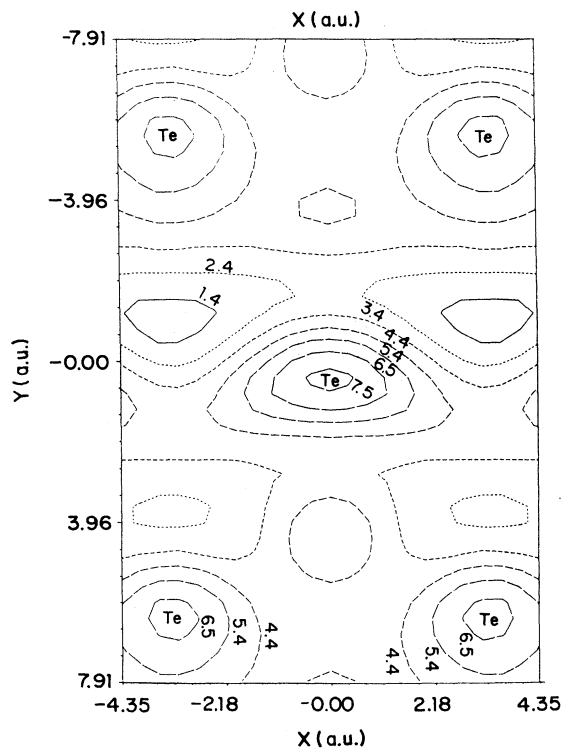

FIG. 4. A total valence charge-density plot of WTe$_2$ calculated with the pseudofunction method. The plot represents the spatial distribution of the surface valence charge density 1.6 Å above the topmost Te plane at the energy $\pm$0.45 eV with respect to the Fermi energy. The charge contours are in relative units.

In conclusion, we have shown from the STM images of WTe_2 that it is possible to image subsurface atoms. The image obtained on this surface is not topographical in origin. It appears that the subsurface W atoms have a higher tunneling probability than the surface Te atoms such that the characteristic zig-zag and slightly buckled chains of W atoms show more clearly in the scanning tunneling micrographs than the surface corrugated Te layer. A first-principles pseudofunction calculation of the surface total valence charge density of this compound cannot explain the STM's preference to image the subsurface atoms, even though similar calculations on the graphite surface were adequate to explain the influence of subsurface atoms on the STM images. A detailed knowledge of the tunneling matrix element might be necessary to explain the experimental observations. The STM results on the WTe_2 suggest that the hexagonal symmetry observed in other transition-metal dichalcogenides such as $2H$-$MoTe_2$, $2H$-MoS_2, and $2H$-$NbSe_2$ are likely due to the metal layer rather than the chalcogenide layer.

ACKNOWLEDGEMENTS

[1]A. A. Balchin, in *Crystallography and Crystal Chemistry of Materials with Layered Structures,* edited by F. Levy (Reidel, Dordrecht, 1976), pp. 1–50; P. M. Williams, *ibid.,* pp. 51–92.

[2]J. L. Stickney, S. D. Rosasco, B. C. Schardt, T. Solomun, A. T. Hubbard, and B. A. Parkinson, Surf. Sci. **136**, 15 (1984).

[3]R. V. Coleman, B. Drake, P. K. Hansma, and G. Slough, Phys. Rev. Lett. **55**, 394 (1985); C. G. Slough, W. W. McNairy, R. V. Coleman, B. Drake, and P. K. Hansma, Phys. Rev. B **34**, 994 (1986); B. Giambattista, A. Johnson, R. V. Coleman, B. Drake, and P. K. Hansma, *ibid.* **37**, 2741 (1988); X. L. Wu and C. M. Lieber, J. Am. Chem. Soc. **110**, 5200 (1988); X. L. Wu, P. Zhou, and C. M. Lieber, Nature (London) **335**, 55 (1988).

[4]K. Uozumi, K. Nakamoto, and K. Fujioka, Jpn. J. Appl. Phys. **27**, L123 (1988); D. C. Dahn, M. O. Watanabe, B. L. Blackford, and M. H. Jericho, J. Appl. Phys. **63**, 315 (1988).

[5]M. Weimer, J. Kramar, C. Bai, and J. D. Baldeschwieler, Phys. Rev. B **37**, 4292 (1988).

[6]G. W. Stupian and M. S. Leung, Appl. Phys. Lett. **51**, 1560 (1987).

[7]D. Sarid, T. Henson, N. R. Armstrong, and L. S. Bell, Appl. Phys. Lett. **52**, 2252 (1988).

[8]H. Bando, N. Morita, H. Tokumoto, W. Mizutani, K. Watanabe, A. Homma, S. Wakiyama, M. Shigeno, K. Endo, and K. Kajimura, J. Vac. Sci. Technol. A **6**, 344 (1988).

[9]B. Brown, Acta Crystallogr. **20**, 268 (1966).

[10]S. L. Tang, R. V. Kasowski, M. A. Subramanian, and W. Y. Hsu, Physica B+C **156C**, 177 (1988).

[11]Nanoscope II, Digital Instrument Inc.

[12]S. L. Tang, B. A. Parkinson, F. Ohuchi, and L. E. Firment (unpublished).

[13]W. G. Dawson and D. W. Bullett, J. Phys. C **20**, 6159 (1987).

[14]R. V. Kasowski (unpublished).

[15]J. Tersoff and D. R. Hamann, Phys. Rev. Lett. **50**, 1998 (1983); Phys. Rev. B **31**, 805 (1985).

[16]I. P. Batra, N. Garcia, H. Rohrer, H. Salemink, E. Stoll, and S. Ciraci, Surf. Sci. **181**, 126 (1987).

[17]G. Binnig, H. Fuchs, Ch. Gerber, H. Rohrer, E. Stoll, and E. Tosatti, Europhys. Lett. **1**, 31 (1986).

[18]R. V. Kasowski and M.-H. Chai, Phys. Rev. Lett. **60**, 546 (1988).

[19]F. Herman, R. V. Kasowski, and W. Y. Hsu, Phys. Rev. B **38**, 204 (1988).

[20]B. Marchon, P. Bernhardt, M. E. Bussel, G. A. Somorjai, M. Salmeron, and W. Siekhaus, Phys. Rev. Lett. **60**, 1166 (1988).

[21]M. D. Pashley, K. W. Haberern, W. Friday, J. M. Woodall, and P. D. Kirchner, Phys. Rev. Lett. **60**, 2176 (1988).

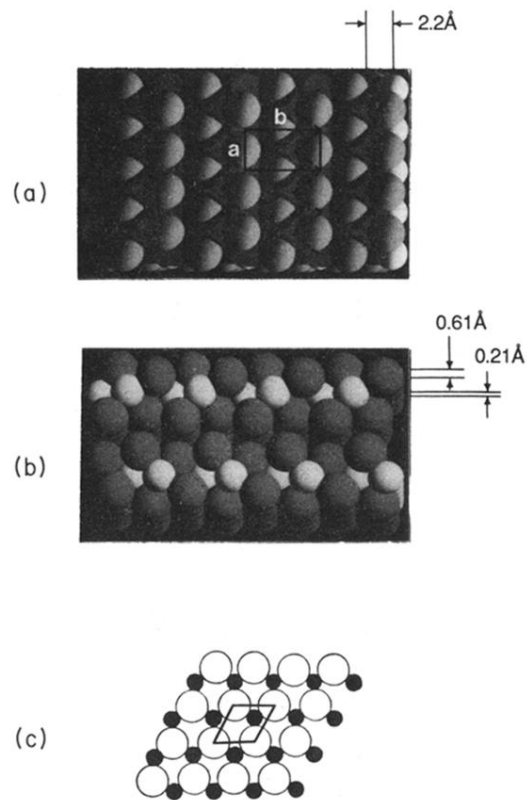[22]R. J. Hamers, R. M. Tromp, and J. E. Demuth, Phys. Rev. Lett. **56**, 1972 (1986).

FIG. 1. (a) A computer model of the WTe_2 surface with shadowing to highlight the corrugated nature of the Te atoms. Dark balls, Te; light balls, W. Surface unit-cell vector $a = 3.5$ Å, $b = 6.3$ Å. The zig-zag chains of tungsten atoms are denoted by the dashed line. (b) A side view of two computer-generated WTe_2 sandwich layers to show the buckling of the paired tungsten rows and the corrugated Te surface layer. (c) The atomic arrangement of the $2H$-$MoTe_2$ surface. Open circle, surface Te; solid circle, subsurface Mo. The nearest-neighbor distance is 3.5 Å.
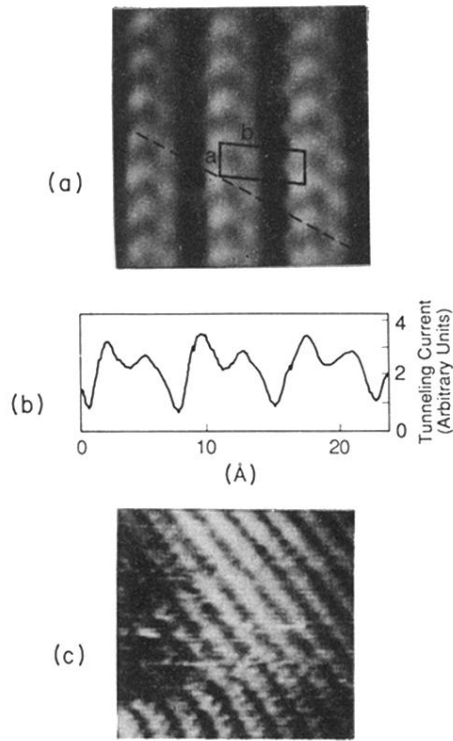
FIG. 2. (a) A (20×25)-$\overset{\circ}{\text{A}}{}^{2}$ constant-height scan of the WTe$_2$ surface. The surface unit cell is outlined. The dashed line shows the location of the cross-section line scan shown in (b). (b) The cross-section line scan through the paired, zig-zag rows in (a). (c) A (50×50)-$\overset{\circ}{\text{A}}{}^{2}$ scan of the WTe$_2$ surface taken with a constant current. Horizontal streaks along the x-scan directions indicate changes in the tip resolution. The zig-zag pattern of the W layer is clearly observed at the lower part of the scan, but no longer distinguishable toward the top of the scan. The dark areas with atomic features superimposed on them on the left of the scan are defects due to oxygen contamination.
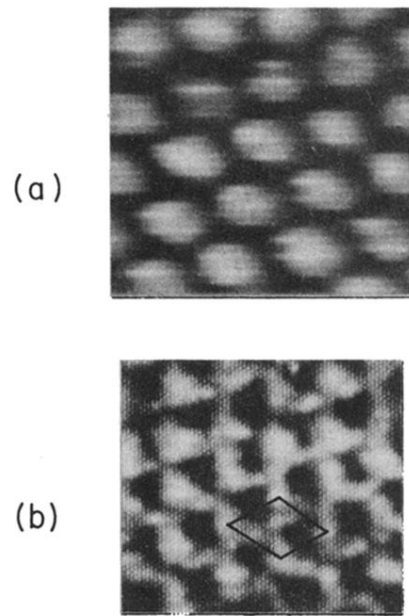
FIG. 3. STM images of the $2H$-MoTe$_2$ surface taken with the constant-current mode. (a) A (15×15)-$\text{\AA}^2$ scan showing the familiar hexagonal symmetry. (b) A (16×16)-$\text{\AA}^2$ scan showing additional features attributable to atoms from a different layer. A unit cell is drawn to show the position of the additional feature.